PESDES 2017
International Workshop on
Performance-Based Seismic Design of Structures
D. Beskos, Y. Zhou, J. Qian, X. Lu (eds.)
Tongji University, Shanghai, China, 13-15 October 2017

EXPERIMENTAL AND NUMERICAL EVALUATION OF STEEL COLUMNS FOR PERFORMANCE-BASED SEISMIC ASSESSMENT OF STEEL MOMENT FRAMES

Dimitrios G. Lignos[1], Ahmed Elkady[1], Yusuke Suzuki[2] and Alexander Hartloper[1]

[1] Ecole Polytechnique Fédérale de Lausanne (EPFL)
address
e-mail: {dimitrios.lignos, ahmed.elkady, alexander.hartloper}@epfl.ch

[2] Nippon Steel and Sumitomo Metal Corporation
address
suzuki.s2k.yusuke@jp.nssmc.com

Keywords: Steel columns, Full-scale testing, Column axial shortening, Nonlinear modeling, Cyclic deterioration.

Abstract. *This paper summarizes the findings of a long term experimental program corroborated with detailed finite element simulations that investigated the hysteretic behavior of wide-flange columns in steel moment-resisting frames (MRFs) designed in highly seismic regions. Several aspects of the steel column behavior are thoroughly investigated. It is shown that steel column axial shortening is a failure mode that strongly influences the steel column stability under earthquake-induced loading. The amount of axial shortening can be considerably different in interior columns compared to end (exterior) columns that experience transient axial load demands due to dynamic overturning effects. Axial shortening is typically followed by column out-of-plane deformations that become maximum near the dissipative plastic hinge zone and migrate near the column top end. This failure mode is strongly influenced by the considered column end boundary conditions. Routinely used symmetric loading histories provide insufficient information for modeling the cyclic deterioration in flexural strength and stiffness of steel columns near collapse. Modeling recommendations for updated backbone parameters for nonlinear modeling of steel columns are proposed inline with the current ASCE 41 nonlinear modeling recommendations for performance-based seismic assessment of steel moment frames.*

1 INTRODUCTION

With the advent of performance-based earthquake engineering, nonlinear modeling of structural components is essential in order to assess the seismic performance of frame buildings from the onset of damage through the occurrence of structural collapse. Historically, the ASCE 41 [1] nonlinear modeling provisions have been employed for this purpose. Limited experimental evidence primarily from small scale wide-shape steel columns (e.g., [2]) suggests that these members may behave much better than expected in reality. However, steel columns in moment resisting frames (MRFs) are subjected to complex cyclic loading. This is due to the randomness of the imposed earthquake loading history, the dynamic overturning effects that impose transient axial load demands to end (exterior) columns compared to interior columns within the same story, as well as the bidirectional loading due to the 3-dimensional ground motion shaking. Other issues associated with the effect of member end boundary conditions have also been overlooked because in most cases steel columns were tested with simplified boundary conditions. In particular, these were either assumed to be fixed-fixed or fixed-free (i.e., cantilever). More recently, the earthquake-induced collapse risk quantification of frame buildings has gained increased attention [3]. In this context, a number of researchers (e.g., [4]) have highlighted the lack of monotonic tests that push structural components far into the inelastic range in order to properly quantify their ultimate deformation capacity.

In order to satisfy all the aforementioned objectives, a 6-year experimental program has been conducted that examined the hysteretic behavior of steel columns subjected to multi-axis cyclic loading. This program was corroborated by detailed finite element simulations that facilitated the expansion of the test results to a wide range of steel column sizes currently used in the seismic design practice. This paper summarizes the main findings of this program as well a proposed modeling recommendations for updating the current ASCE-41 [1] nonlinear modeling provisions for steel columns in new and existing steel MRFs.

2 TEST MATRIX

The test matrix including the geometric and loading parameters of the test specimens is summarized in *Table 1*. It consists of five sets of cross-section sizes including deep (W16 and W24) as well as shallow cross-sections (i.e., W14). Each set includes a number of nominally identical steel columns fabricated by ASTM A992 Grade 50 steel (i.e., nominal yield stress, f_y = 345MPa). The test specimens are selected by considering (a) the local slenderness ratios of highly compact cross-sections as per AISC 341-10 [5]; and (b) commonly used cross-sections in typical mid-rise steel frame buildings with MRFs. The specimens are tested in two separate testing facilities that are shown in figure 1. At Ecole Polytechnique Montréal (EPM), members are tested in full length (i.e., approximately 4.5m) in a 6-degree-of-freedom-system (see figure 1a) such that the effects of (a) member slenderness; (b) boundary effects; and (c) the bidirectional loading on the column performance can be assessed. At the Jamieson Structures Laboratory (McGill University), steel columns are tested in a cantilever fashion (see figure 1b). In this case, emphasis is placed on the influence of local slenderness, the transient axial load and the influence of loading history on the steel column hysteretic performance.

In brief, nominally identical specimens from different sets are subjected to a range of constant compressive axial load ratios, P_g/P_{ye} = 0.3 and 0.5 (in which, P_g is the gravity load that is applied to the column and P_{ye} is the expected axial yield strength of the respective steel cross-section) coupled with monotonic and/or cyclic lateral loading. In order to investigate the effect of the lateral loading history on the steel column behavior, several specimens are subjected to a collapse-consistent loading protocol that represents the ratcheting behavior of a

column in a steel MRF that approaches collapse [6]. In order to investigate the effect of high axial load demands on the steel column plastic deformation, the W14x82, W16x89 and W24x146 test specimens are subjected to excessive axial compressive ratios P_g/P_{ye} = 0.5 (i.e., P_g/P_{cr} > 0.5; in which P_{cr} is the critical load of a column). Finally, in order to further investigate the differences of the hysteretic response between interior and end columns, several specimens are subjected to varying axial load demands synchronized with the AISC symmetric and a collapse-consistent lateral loading protocol [6]. Referring to table 1, a steel column can be subjected to high axial compressive loads (i.e., $0.75P_{ye}$) as well as relatively high axial tensile loads (i.e., $-0.20P_{ye}$) after the gravity offset is applied. Finally, in order to assess the boundary condition effects on the steel column hysteretic behavior, nominally identical specimens (i.e., W24x146 and W24x84) are considered with both fixed and flexible top end boundaries.

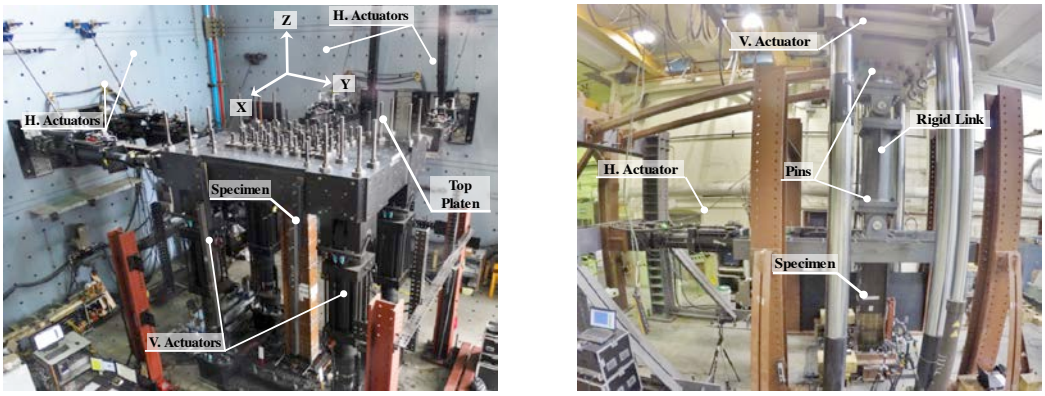

(a) 6-DOF test setup at EPM (b) multi-axis column test simulator at McGill

Figure 1: Experimental setup for steel column testing.

Specimen ID	Cross-	Lateral loading protocol	Axial loading
A-C1	W24x146	AISC-symmetric (fixed-fixed)	P_g/P_{ye} = 0.2
A-C2		AISC-symmetric (fixed-fixed)	P_g/P_{ye} = 0.5
A-C3		AISC-symmetric (fixed-flexible)	P_g/P_{ye} = 0.2
A-C4		Collapse-consistent (fixed-flexible)	P_g/P_{ye} = 0.2
A-C5		Bidir.-symmetric (fixed-flexible)	P_g/P_{ye} = 0.2
A-C6		Bidir.-Collapse-consistent (fixed-flexible)	P_g/P_{ye} = 0.2
A-C7	W24x84	AISC-symmetric (fixed-flexible)	P_g/P_{ye} = 0.2
A-C8		Collapse-consistent (fixed-flexible)	P_g/P_{ye} = 0.2
A-C9		Bidir.-symmetric (fixed-flexible)	P_g/P_{ye} = 0.2
A-C10		Bidir.-Collapse-consistent (fixed-flexible)	P_g/P_{ye} = 0.2
B-C11	W14X53	Monotonic	P_g/P_{ye} = 0.3
B-C12		AISC-symmetric	P_g/P_{ye} = 0.3
B-C13		Collapse-consistent #1	P_g/P_{ye} = 0.3
B-C14		Collapse-consistent #1	Varying
B-C15		Collapse-consistent #2	P_g/P_{ye} = 0.3
B-C16		Collapse-consistent #2	Varying
C-C17	W14x61	Monotonic	P_g/P_{ye} = 0.3
C-C18		Monotonic	P_g/P_{ye} = 0.5
C-C19		Collapse-consistent	P_g/P_{ye} = 0.5
C-C20		AISC-symmetric	Varying
C-C21		AISC-symmetric	P_g/P_{ye} = 0.3

C-C22		Collapse-consistent #1	$P_g/P_{ye} = 0.3$
C-C23		Collapse-consistent #1	Varying
D-C24	W14x82	Monotonic	$P_g/P_{ye} = 0.3$
D-C25		Monotonic	$P_g/P_{ye} = 0.5$
D-C26		AISC-symmetric	$P_g/P_{ye} = 0.5$
D-C27		AISC-symmetric	$P_g/P_{ye} = 0.75$
D-C28		AISC-symmetric	$P_g/P_{ye} = 0.3$
D-C29		Collapse-consistent #1	$P_g/P_{ye} = 0.3$
D-C30		Collapse-consistent #1	Varying
E-C31	W16x89	Monotonic	$P_g/P_{ye} = 0.3$
E-C32		Monotonic	$P_g/P_{ye} = 0.5$
E-C33		AISC-Symmetric	$P_g/P_{ye} = 0.5$
E-C34		AISC-Symmetric	Varying

Table 1: Summary of test matrix for experimental testing of wide flange steel columns.

3 TEST RESULTS AND DISCUSSION

This section discusses a number of findings from the experimental program outlined in Section 2. Emphasis is placed on the effect of boundary conditions, the bidirectional lateral loading, the transient axial load demands and the lateral loading history on the overall steel column stability under cyclic loading. Several other findings can be found in great detail in prior publications by the authors [7-10].

3.1 Influence of boundary conditions on column behavior

Referring to table 1, Series-A tests examined the effect of member end boundary conditions on the column cyclic behavior. This effect is examined by comparing the performance of the two column specimens, A-C1 and A-C3. Specimen A-C1 was tested with a rotationally-fixed top end while specimen A-C3 had a rotationally-flexible top end. The latter is a realistic representation of the flexible rotational stiffness of beam-to-column connections intersecting first story steel MRF columns at their top end. Figure 2a shows that both specimens exhibited very similar moment-rotation behavior at their base; yet, the onset of local buckling occurred a bit later in specimen A-C3, due to its larger flexibility. Referring to Figure 2b, the difference in behavior at the column top between the two specimens is appreciable. While specimen A-C1 experienced larger amount of plastic deformation and strength deterioration at its top end (similar to the column base), specimen A-C3 experienced limited amount of plastic deformation (≈1.5%) as it yielded later during the imposed loading history. The latter is representative of capacity-designed first-story MRF columns that are expected to yield only at their base.

At drifts less than 3%, specimen A-C1 experienced larger out-of-plane deformations near the plastified dissipative zones at the member ends as well as larger twisting angles along its height compared to specimen A-C3. This is attributed to the simultaneous loss of flexural and torsional stiffness at both column ends in specimen A-C1 at relatively smaller drifts [10]. At drifts larger than 3%, the out-of-plane deformations, concentrated only at the base of specimen A-C3, increased rapidly due to the increasing weak-axis member P-Delta demands. This is shown in figure 2c. In particular, the out-of-plane deformations and twisting angles of specimen A-C3 became almost double of those measured in specimen A-C1. These deformations are expected to be amplified in slender columns (i.e., member slenderness ratios, L_b/r_y larger than $L_b/r_y > 80$). In summary, this highlights that the expected column failure mode, and its associated performance can be misleading if fixed-end boundary conditions are considered.

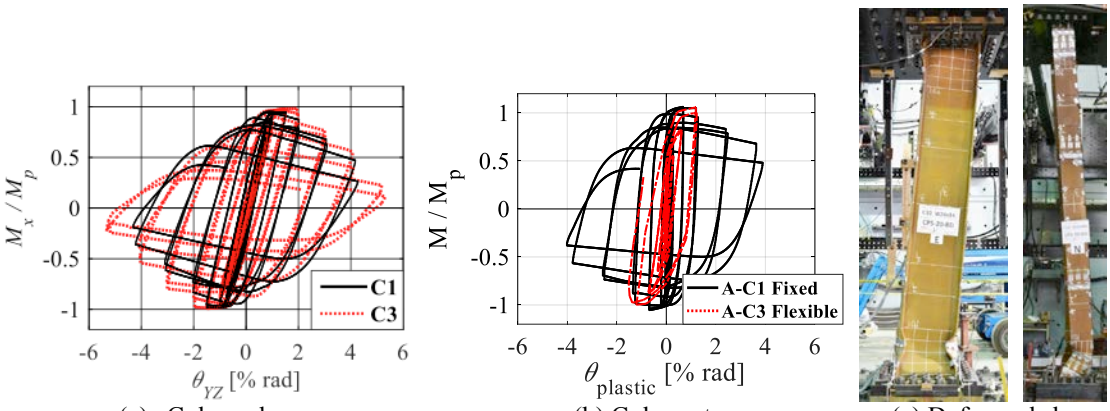

(a) Column base (b) Column top (c) Deformed shape

Figure 2: Effect of column end boundary conditions on the steel column performance.

3.2 Influence of bidirectional loading on steel column behavior

Pair specimens A-C8 - A-C10 and A-C7 – A-C9 utilized the same cross-sections, boundary conditions, and applied axial compressive load (see table 1). The hysteretic behavior of the two specimens is compared in terms of their deduced moment-rotation relation in figure 3. From the same figure, the plastic deformation capacity of a column is practically not sensitive to the bidirectional lateral loading. This observation holds true for the range of sections that were tested regardless of the type of lateral loading (i.e., symmetric or collapse-consistent). Nonetheless, for story drift-ratios larger than 3% radians, the rate of cyclic deterioration in flexural strength of a column is slightly larger under bidirectional lateral loading compared to that from unidirectional lateral loading. This is attributed to the additional flexural demands in the weak-axis direction of the column cross section. This effect is practically negligible on the first-cycle envelope curves of nominally identical specimens. If the objective is to construct a first-cycle envelope curve for a steel column for the nonlinear seismic evaluation of steel MRFs this can be done with experimental data based on unidirectional loading protocols.

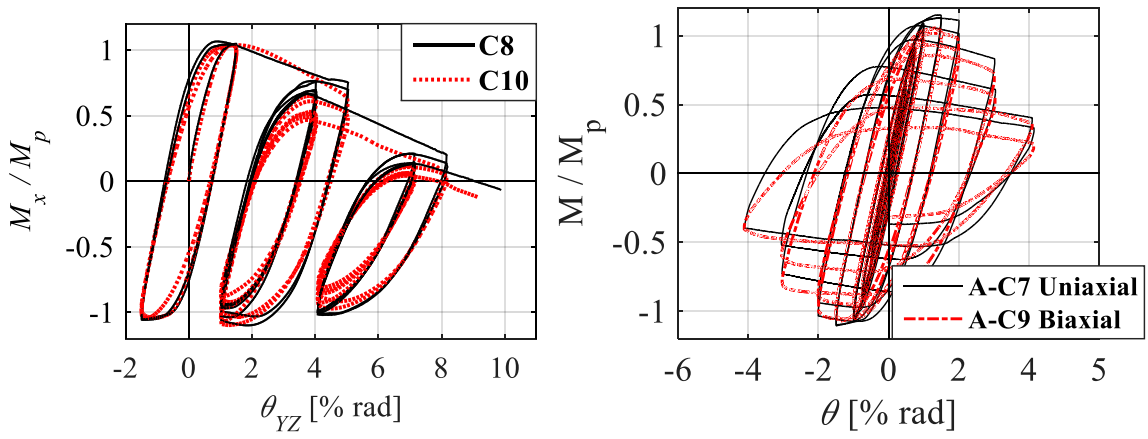

Figure 3: Effect of bidirectional versus unidirectional lateral loading histories on steel column performance.

3.3 Effect of lateral loading history

Figure 4 compares the deduced moment versus chord rotation of the W14x53 specimens, respectively, under various lateral loading protocols (i.e., Specimens B-C11 to B-C14). From this figure, the flexural strength deterioration of this column became zero at chord rotations larger than 15% based on the monotonic backbone curve. In addition, the flexural strength of

a test specimen deteriorated in the positive and negative loading direction when the axial load was kept constant. This is due to the formation of local buckling in both flanges of a steel column. Note that when varying axial load is coupled with lateral drift demands then the flexural strength of a steel column does not typically deteriorate in the negative loading direction. This is due to the position of the cross-sectional neutral axis. Therefore, it is expected that interior steel columns would typically lose faster their flexural strength and axial load carrying capacity compared to end columns within the same MRF story.

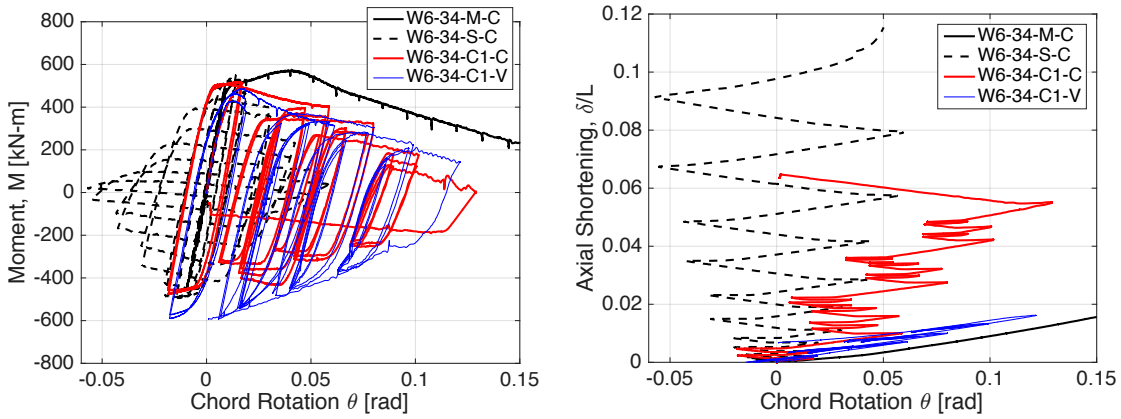

(a)Moment-rotation (b)Axial shortetning-rotation

Figure 4: Effect of lateral loading history on steel column stability.

Referring to figure 4, when a symmetric cyclic lateral loading protocol is employed the steel column flexural strength deteriorates a lot faster than a nominally identical specimen that experiences a collapse-consistent loading protocol. This is due to the large number of inelastic loading cycles included in a symmetric cyclic lateral loading protocol. However, columns in steel MRFs subjected to ordinary or near-fault ground motions would typically experience few inelastic cycles followed by a large monotonic push prior to structural collapse [4,6,9]. Prior studies associated with the collapse assessment of frame buildings have highlighted that the pre- and post-capping plastic rotation capacities are fundamental quantities for the reliable collapse assessment [4, 11]. Referring to figure 4a, these become available only when a combination of a monotonic and a collapse-consistent lateral loading protocol is employed for experimental testing of steel columns. Same findings hold true for all the tested specimens.

Figure 4b illustrates the steel column axial shortening versus chord rotation relations for the same specimens discussed previously. The axial shortening is normalized with respect to the respective column height. Referring to figure 4b, when a constant compressive axial load is applied on a steel column, its axial shortening accumulates in both the positive and negative loading directions. The amount of axial shortening depends on the number of inelastic loading cycles of the respective lateral loading protocol as well as the applied axial load. Referring to figure 4b, end columns would experience 6 to 7 times smaller axial shortening compared to interior columns. The reason is that end columns experience tensile load demands in the negative loading direction due to dynamic overturning effects. To limit the amount of column axial shortening an obvious solution can be the reduction of the local slenderness limits for highly ductile members [12].

4 FINITE ELEMENT MODELING

In parallel with the experimental program, an extensive finite element (FE) parametric study was conducted. To this end, a detailed finite element modeling approach was utilized. The modeling approach considers material nonlinearity and residual stresses commonly found

in hot-rolled sections. The FE modeling approach was validated with the experimental data from the full-scale testing program discussed earlier. A sample comparison of the deduced moment-rotation and axial displacement-rotation relations and the ones predicted by FE analysis is shown in figures 5a and 5b, respectively. A sample comparison of the local deformation profiles between tests and FE models are shown in figure 5c. More details can be found in [8, 12]. Overall, the FE modeling approach is able to capture with reasonable accuracy the nonlinear behavior of steel columns regardless of the employed cross-section, geometry, boundary conditions and the applied loading protocol. To assess the behavior of a "bigger pool" of cross-sections used in the current seismic deign practice, more than 40 cross-sections ranging from W12 to W36 were examined [12]. Emphasis is placed on stocky (set W1), moderately stocky (set W2), slender but highly ductile (set W3) and moderately compact (set W4) cross sections. The aim was to refine the current seismic design standards as well as to propose updated nonlinear modeling recommendations for steel columns in steel MRFs.

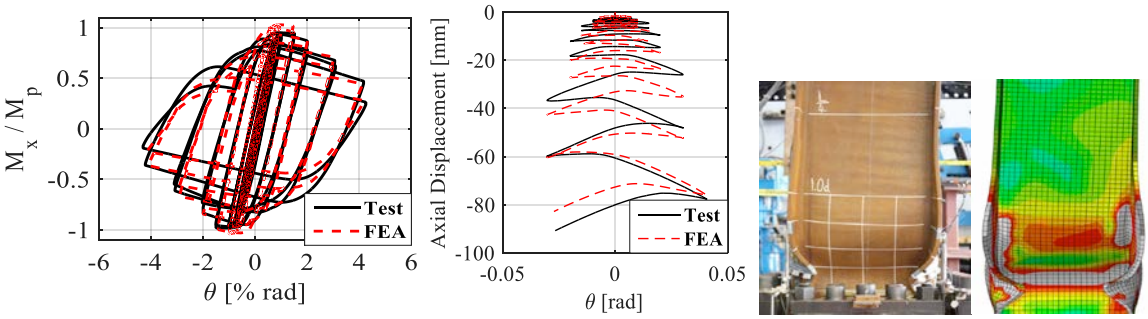

(a)Moment rotation (b) axial shortening – rotation (c) deformed shape

Figure 5: Finite element model validation with experimental data.

5 DEVELOPMENT OF NONLINEAR MODELING RECOMMENDATIONS FOR STEEL COLUMNS

Figure 6 shows the multi-linear component model used in the proposed recommendations. In the same figure, the current ASCE-41-13 [1] component model is superimposed. The variables Q and Δ represent the steel column flexural strength, M, and the chord rotation, θ, respectively. In this figure, the blue curve represents the monotonic curve of a steel column, which is considered to be a unique property of a structural component. The red line represents the first-cycle envelope curve of a steel column subjected to a reversed cyclic symmetric loading history. Although this curve is loading history dependent, practicing engineers use it in nonlinear static analysis procedures to inherently capture the cyclic deterioration in strength and stiffness of structural components subjected to a consistent cyclic loading protocol.

The effective elastic stiffness, K_e, should consider both flexure and shear deformations. Assuming double curvature in the column, the effective elastic flexural stiffness is:

$$K_e = \frac{K_s \cdot K_b}{K_s + K_b} \cdot \frac{L^2}{2},\ K_s = GA_w / L,\ K_b = 12EI / L^3 \tag{1}$$

In which K_s is the stiffness of the column considering shear deformations only, and K_b is the stiffness considering flexure only; G is the shear modulus of the steel material; A_w is the area of the web; L is the length of the column; E is the elastic modulus of the steel material; and I is the moment of inertia of the column. The effective yield strength, Q_y^* is:

$$M_y^* = \begin{cases} 1.15 \cdot Z \cdot R_y \cdot F_y (1 - P_g / 2P_{ye}) & \text{if } P_g / P_{ye} \le 0.20 \\ 1.15 \cdot Z \cdot R_y \cdot F_y [9/8(1 - P_g / P_{ye})] & \text{if } P_g / P_{ye} > 0.20 \end{cases} \tag{2}$$

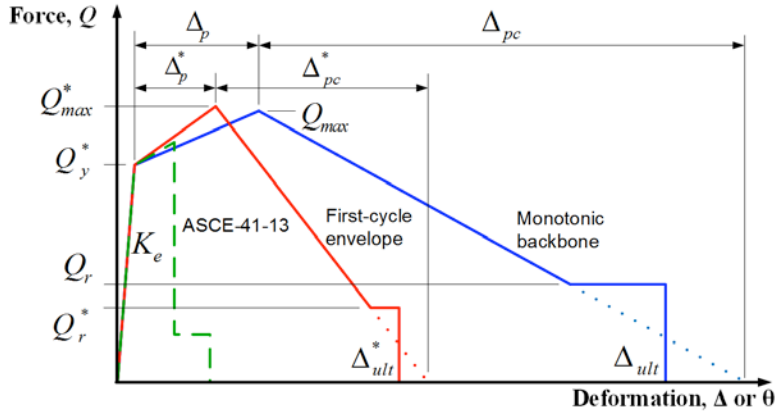

Figure 6: Proposed component model and comparison with ASCE-41 component model.

for Equation 2, the COV = 0.10. In which, P_g is the column axial load due to gravity; P_{ye} is the expected axial yield strength; Z is the plastic section modulus of the column; R_y is a factor to obtain the expected yield stress from Table A3.1 per AISC-341-10 [5]; and F_y is the nominal yield stress of the respective steel material. Equation 2 is based on the AISC interaction equations, where the 1.15 factor accounts for the effects of cyclic hardening on the column flexural strength. For the following equations, the superscript asterisk (*) denotes the equations used for the first-cycle envelope, while the absence of the asterisk denotes the equations to be used for the monotonic backbone.

Peak (capping) strength, Q_{max} or Q^*_{max}: $M_{max} = aM^*_y$, or $M^*_{max} = a^*M^*_y$ where,

$$a = 12.5\left(\frac{h}{t_w}\right)^{-0.2}\left(\frac{L_b}{r_y}\right)^{-0.4}\left(1-\frac{P_g}{P_{ye}}\right)^{0.4} \geq 1.0, (COV = 0.10) \quad (3)$$

$$a^* = 9.5\left(\frac{h}{t_w}\right)^{-0.4}\left(\frac{L_b}{r_y}\right)^{-0.16}\left(1-\frac{P_g}{P_{ye}}\right)^{0.2} \geq 1.0, (COV = 0.07) \quad (4)$$

In Equations 3 and 4, if $P_g/P_{ye} > 0.3$, or if $h/t_w < 15$, then a (or a^*) ≤ 1.3.

Pre-peak plastic deformation, Δ_p or Δ^*_p:

$$\theta_p = 294\left(\frac{h}{t_w}\right)^{-1.7}\left(\frac{L_b}{r_y}\right)^{-0.7}\left(1-\frac{P_g}{P_{ye}}\right)^{1.6} \leq 0.20, (COV = 0.39) \quad (5)$$

$$\theta^*_p = 15\left(\frac{h}{t_w}\right)^{-1.6}\left(\frac{L_b}{r_y}\right)^{-0.3}\left(1-\frac{P_g}{P_{ye}}\right)^{2.3} \leq 0.10, (COV = 0.31) \quad (6)$$

Post-peak plastic deformation, Δ_{pc} or Δ^*_{pc}:

$$\theta_{pc} = 90\left(\frac{h}{t_w}\right)^{-0.8}\left(\frac{L_b}{r_y}\right)^{-0.8}\left(1-\frac{P_g}{P_{ye}}\right)^{2.5} \leq 0.30, (COV = 0.26) \quad (7)$$

$$\theta_{pc}^{*} = 14\left(\frac{h}{t_w}\right)^{-0.8}\left(\frac{L_b}{r_y}\right)^{-0.5}\left(1-\frac{P_g}{P_{ye}}\right)^{3.2} \leq 0.10, (COV = 0.42) \tag{8}$$

Residual strength, Q_r or Q_r^*:

$$M_r = \left(0.5 - 0.4\frac{P_g}{P_{ye}}\right)M_y^*, (COV = 0.27) \tag{9}$$

$$M_r^* = \left(0.4 - 0.4\frac{P_g}{P_{ye}}\right)M_y^*, (COV = 0.35) \tag{10}$$

Ultimate deformation, Δ_{ult} or Δ_{ult}^*:

$$\theta_{ult} = 0.15\,\text{rads}, (COV = 0.46);\ \theta_{ult}^* = 0.08(1 - 0.6P_g / P_{ye})\,\text{rads}, (COV = 0.51) \tag{11}$$

The geometric limits on Equations 2 through 11 are:

$$3.71 \leq h/t_w \leq 57.5\ \ 1.82 \leq b_f / 2t_f \leq 8.52\ \ 38.4 \leq L_b / r_y \leq 120$$

Equations 2 to 12 are developed for ASTM A992 Grade 50 (F_y = 345 MPa) steel. Additionally, columns with $P_g/P_{ye} > 0.60$ that have $h/t_w > 43$ and $KL/r_y > 120$ should be treated as force-controlled as per ASCE-41-13 [1]. This agrees with recent findings by Bech et al. [13].

6 CONCLUSIONS

This paper presents a summary of the many findings related to the hysteretic behavior of steel columns under multi-axis cyclic loading. The assessment is based on a coordinated experimental and numerical program that investigated the influence of several parameters on the steel column stability under cyclic loading. The findings underscore the influence of the member end boundary conditions, the lateral loading history, the bidirectional versus unidirectional loading on the overall column performance. Improvements to the nonlinear modeling of wide-flange columns in conventional steel frame seismic force resisting systems are also presented. The gathered test data, supported by results from detailed finite element studies, is analyzed using multiple regression analysis. From this, empirical relations are derived between the column's plastic deformation and post-yield hardening parameters, and the model input variables. Guidance is provided for the development of component models for both nonlinear static and dynamic analysis procedures. The proposed equations predict the monotonic and first-cycle envelope curves of wide-flange steel columns experiencing deterioration mechanisms under combined axial loading and lateral drift demands and provide an improvement of the current ASCE-41 component models for steel columns. These recommendations facilitate the seismic assessment of steel MRFs within the performance-based earthquake engineering framework.

ACKNOWLEDGMENTS

This study was based on work supported by the National Science and Engineering Research Council of Canada under the Discovery Grant Program. Funding was also provided by the Canadian Institute of Steel Construction and the Swiss National Science Foundation (Award

No. 200021_169248). This financial support is gratefully acknowledged. Any opinions, findings, and conclusions or recommendations expressed in this paper are those of the authors and do not necessarily reflect the views of sponsors.

REFERENCES

[1] ASCE, *Seismic evaluation and retrofit of existing buildings*. ASCE/SEI-41-13, 2014.

[2] E. Popov, V.V. Bertero, S. Chantramouli, Hysteretic behavior of steel columns. *Report UCB/EERC-75-11*, Earthquake Engineering Research Center (EERC), University of California, Berkeley, 1975.

[3] FEMA, *Quantification of building seismic performance factors*. Report FEMA-P695, 2009.

[4] D.G. Lignos, H. Krawinkler, A.S. Whittaker, Prediction and validation of sidesway collapse of two scale models of a 4-story steel moment frame. *Earthquake Engineering & Structural Dynamics*, Vol. **40(7),** 807-825, 2011.

[5] AISC. *Seismic provisions for structural steel buildings*. ANSI/AISC 341-10, Chicago, IL: American Institute for Steel Construction, 2010.

[6] Y. Suzuki, D.G. Lignos, Development of loading protocols for experimental testing of steel columns subjected to combined high axial load and lateral drift demands near collapse. EERI ed. *10th National Conference on Earthquake Engineering*, Anchorage, Alaska, 2014.

[7] A. Elkady, D.G. Lignos, Dynamic stability of deep slender wide-flange steel columns-full scale experiments. SSRC ed. *SSRC Annual Stability Conference, Structural Stability Research Council,* Orlando, Florida, 2016.

[8] A. Elkady, D.G. Lignos. Stability requirements of deep steel wide-flange columns under cyclic loading. SSRC ed. *SSRC Annual Stability Conference, Structural Stability Research Council*, San Antonio, Texas, 2017.

[9] Y, Suzuki, D.G. Lignos. Large scale collapse experiments of wide flange steel beam-columns. *8th International Conference on Behavior of Steel Structures in Seismic Areas* (STESSA), Shanghai, China, 2015.

[10] A. Elkady, D.G. Lignos. Full-scale testing of wide-flange steel columns under multi-axis cyclic loading: Loading sequence, boundary effects and out-of-plane brace force demands. *ASCE Journal of Structural Engineering*, 2017 (in press).

[11] L.F. Ibarra, H. Krawinkler. Global collapse of frame structures under seismic excitations. PEER ed. *Report No. PEER 2005/06*, Pacific Earthquake Engineering Research Center, 2005.

[12] A. Elkady, D.G. Lignos. Analytical investigation of the cyclic behavior and plastic hinge formation in deep wide-flange steel beam-columns. *Bulleting of Earthquake Engineering*, 13(4), 1097-1118, 2015.

[13] D. Bech, B. Tremayne, J. Houston. Proposed changes to steel column evaluation criteria for existing buildings. ATC ed. *2nd ATC-SEI Conference on Improving the Seismic Performance of Existing Buildings and Other Structures*, San Francisco, CA, USA, 2015.